

Nanoparticle Spectroscopy: Plasmon Coupling in Finite-Sized Two-Dimensional Arrays of Cylindrical Silver Nanoparticles

Jiha Sung, Erin M. Hicks, Richard P. Van Duyne,* and Kenneth G. Spears*

Chemistry Department, Northwestern University, Evanston, Illinois 60208-3113

Received: September 12, 2007; In Final Form: December 24, 2007

This study provides new data for interpreting plasmon coupling in finite two-dimensional arrays, which are important in plasmonic devices and sensing applications. Finite square arrays of cylindrical silver nanoparticles with two different nanoparticle diameters (339 and 163 nm) and two different interparticle spacings (400 and 450 nm) were fabricated by e-beam lithography. The plasmonic properties of these arrays were obtained by UV–visible–near-IR extinction spectroscopy and compared with isolated particle spectra. In the case of the large-diameter particle arrays, the semi-infinite array resonance is quite blue-shifted from the isolated particle resonance; the resonant wavelength of the 2×2 particles and successively larger blocks keeps blue-shifting relative to the isolated particle resonance and converges to that of a semi-infinite array. For the small-diameter particle arrays, the semi-infinite resonance is red-shifted from the isolated particle resonance; the resonant wavelength of the 2×2 particles and successively larger blocks keeps red-shifting and converges to the semi-infinite array. The experimental resonances for progressively increasing array sizes show systematic resonance shifts consistent with increasing numbers of particles, and the bandwidth trends require models and more experiments to obtain better insight into trends.

I. Introduction

The optical properties of nanofabricated noble metal nanoparticles have drawn particular interest because of their importance in applications including bio/chemosensors,^{1–4} optical filters,^{5,6} plasmonic waveguides,^{7–10} and substrates for surface-enhanced spectroscopy.^{11–13} The unique optical properties of the nanoparticles that are distinguished from those of bulk originate from the localized surface plasmon resonance (LSPR), which is a collective oscillation of the conduction electrons that occurs when light impinges on a nanoparticle at a specific wavelength. The LSPR can be controlled by changing the size, shape, composition,^{14–16} and dielectric environment of the nanoparticle.^{17,18} In the case of nanoparticle clusters and nanoparticle arrays, electromagnetic coupling between nanoparticles is also an important factor that determines the overall plasmon resonance of the system.

Two adjacent nanoparticles with various particle spacing have been fabricated by electron beam lithography (EBL) and their optical properties have been explored by various research groups.^{19–24} They monitored the resonance wavelength of the system while the particle spacing was tuned and they observed that, for incident beam polarization parallel to the array axis (longitudinal excitation), the resonance of the system red-shifts as particles get closer, while for incident beam polarization perpendicular to the array axis (transverse excitation), the resonance blue-shifts as particles get closer. Those observations also have been explained by various theoretical models,^{21,24–27} which provide insight into the relative importance of dipole–dipole interactions and near-field interactions. A molecular ruler utilizing this sensitivity of LSPR to the particle spacing has been demonstrated by Alivisatos and co-workers.^{28,29}

The optical properties of more extended systems, such as one-dimensional (1D)^{30–32} and two-dimensional (2D)^{33–36} semi-infinite arrays, have been studied experimentally and their observations were rationalized by theoretical studies.^{37–41} Particle spacing and incident beam polarization dependence was studied for various shapes of nanoparticles. Aussenegg and co-workers^{33,34} have studied grid-spacing-dependent extinction spectra and plasmon lifetimes of 2D gold cylinder and nanorod arrays. Van Duyne and co-workers studied short-range coupling effects in hexagonal and square arrays of triangular and cylindrical gold and silver nanoparticles,³⁶ and Schatz and co-workers studied those optical properties theoretically by T-matrix, coupled dipole (CD) approximation, and discrete dipole approximation (DDA) methods.^{36,40,42} Grid-spacing-dependent extinction spectra of 2D L-shaped nanoparticle arrays was also studied by Spears and co-workers.³⁵

The effect of the number of nanoparticles on the plasmon resonance has been studied on a finite 1D chain with small numbers of nanoparticles. Atwater and co-workers⁴¹ measured the far-field extinction spectra of a 1D chain of cylindrical gold nanoparticles with illumination for both longitudinal and transverse polarization. The number of nanoparticles in a single chain was varied from 3 to 80 particles, and they observed that the plasmon resonance red-shifts monotonically for longitudinal excitation and blue-shifts for transverse excitation as the number of nanoparticles was increased. They also performed finite-difference time-domain (FDTD) simulations⁴¹ and three-dimensional full-field electromagnetic simulations³¹ for their system and verified their results. On the other hand, Zhang and co-workers⁴³ studied a 1D chain of 1–6 gold nanoparticles experimentally and theoretically, and they observed nonmonotonic behavior of the plasmon resonance shift for the condition where the phase retardation effect affects the resonance wavelength. Bouhelier et al.⁴⁴ studied the effect of particle size, grid

* To whom correspondence should be addressed: e-mail k-spears@northwestern.edu (K.G.S.) or vanduyne@northwestern.edu (R.P.V.D.).

spacing, and number of particles on the resonant wavelength and bandwidth of a 1D chain of gold nanoparticles.

In the case of finite 2D arrays with a small number of nanoparticles, Ng and Liu⁴⁵ theoretically modeled the optical properties of 2×3 (six particles arranged in two rows and three columns) arrays of cylindrical nanoparticles with fixed interparticle distance and variable particle size. However, there have been no experimental studies on how the number of nanoparticles affect the optical properties of finite 2D arrays, other than our work on 2D L-shaped nanoparticles for one particle size and grid spacing.³⁵

Theoretical insight into the relative importance of near- and far-field (dipole–dipole) coupling provides insight into the controlling interactions for given particle sizes and spacings in arrays.^{21,24} A common observation of these studies is that the spectral shift (in nanometers) normalized by the peak wavelength has an exponential decay of $a \exp(-x/b)$ with the parameter $x = s/d$, where s is the interparticle gap and d is the particle diameter. Decay constants for gold²⁴ of $b = 0.23$ and for silver²¹ of $b = 0.22$ have been found in experiment and theory; a depends on the metal. The origin of these shifts at larger separations is dipole–dipole interaction, and the onset of other interactions is clearly apparent at values of $x < 0.2$ due to multipolar fields and finite size effects. By comparison of DDA models with full electric field effects and coupled-dipole models, prior work has attempted to identify when near-field coupling effects become important.^{21,24} The graphical plots of these two models are both nominally exponential but with different decay constants, so that absolute accuracy would be required to compute the relative contributions of each model. This continuous behavior prevents a simple statement as to when long-range dipole coupling is being distorted by near-field coupling effects, but one group²¹ has suggested that a gap value $s < 20$ nm for experimental values of $x = 0.13$ – 0.17 is a region where the near-field effects are large. In our work we have a large diameter particle ($d = 339$ nm) and a small diameter particle ($d = 163$ nm), and only the large diameter particle of 339 nm has spacings that begin to show near-field coupling effects at $x = 0.18$. The systematic changes in array resonances that we find experimentally are consistent with prior work that shows dominance of dipole–dipole coupling in arrays.^{21,33,36,40}

In this paper, we extend the study of the plasmonic properties of two-dimensional square arrays to the case of finite arrays. Finite arrays with two different nanoparticle diameters (339 and 163 nm) and two different interparticle spacings (400 and 450 nm) were fabricated by EBL. Their optical properties were obtained by far-field, UV–vis–near-IR extinction spectroscopy and were compared with that of both isolated nanoparticles and semi-infinite 2D arrays. The motivation for this study was to elucidate the plasmon coupling effects on wavelength and bandwidth in finite nanoparticle arrays. From the above discussion, we expect that the both size particles are dominated by dipole–dipole coupling, with some contribution from near-field coupling for the large particles, which also have larger dipoles than the small particles. It is anticipated that finite arrays will play an important role in both future plasmonic devices and multiplex sensing platforms for chemical and biological analytes. For example, in order to fabricate a LSPR sensor chip with a 4×6 array of independent pixels analogous to the imaging surface plasmon resonance (SPR) chips developed by Corn and co-workers,⁴⁶ it is essential to know how many nanoparticles/pixel are required to get both narrow LSPR line width and a predetermined LSPR wavelength. Systematic studies of the type

presented here and additional theoretical models are required to achieve this design goal.

II. Experimental Methods

A. Sample Fabrication and Structural Characterization.

The nanoparticle arrays were fabricated on an indium–tin oxide (ITO) conducting layer of 40 nm on a $750 \mu\text{m}$ thick glass substrate by EBL. Each sample was fabricated over the area of $100 \times 100 \mu\text{m}^2$ and they were separated by 1 or 2 mm. As a guide for finding samples, $50 \times 50 \mu\text{m}^2$ and $500 \times 500 \mu\text{m}^2$ silver films were fabricated by photolithography as markers within each sample and at the beginning and ending of each row of samples. Samples were fabricated at the Michigan Nanofabrication Facility (MNF), which is part of the National Nanotechnology Infrastructure Network (NNIN).

Exposure of the patterns was done in a two-step process: marker fabrication by photolithography and sample fabrication by EBL. In the first step, the markers were fabricated on the substrate by photolithography. The substrate was prebaked at 130°C for 10 min to remove any excess moisture on the surface, and a resist, S1813 (Microchem), was spun on the surface at 4000 rpm for 30 s. A post-spin bake at 115°C for 60 min was then performed. The mask was then exposed for 6 s in a MA-6 aligner. The pattern was developed in MIF 319 (Microchem) for 30 s, rinsed in water, and dried in nitrogen. The substrate was then mounted in a Cooke evaporator and 30 nm of silver was deposited. Excess resist was removed via an overnight soak in acetone. Subsequent preparation of the nanoparticle arrays by EBL was performed as the second step. A resist, 950k PMMA A4 (Microchem), was spun onto the existing pattern (markers) at 4000 rpm for 45 s, and the substrate was then soft-baked at 170°C overnight. A RAITH 150 was used to expose the resist, employing an accelerating voltage of 20 kV, aperture of $20 \mu\text{m}$, and a working distance of 7 mm. After the exposure, the sample patterns were then developed for 2 min in a 3:1 mixture of isopropyl alcohol (IPA) and methyl isobutyl ketone (MIBK) to create areas for deposition of silver. Silver (30 nm) was then deposited (Cooke evaporator) over both the pattern and resist and subsequently removed, leaving patterned nanoparticles behind. This was accomplished by slightly overdeveloping the resist.

Scanning electron microscopic (SEM) images of the nanoparticle shape and array structure are shown in Figure 1. SEM imaging was performed in the EPIC center at Northwestern University with a Hitachi 4500. The diameter (d) of the nanoparticles is 339 ± 6 nm for large cylinders (Figure 1A) and 163 ± 4 nm for small cylinders (Figure 1B). The height of cylinders is 30 nm. Two different types of arrays were fabricated for both large and small cylinders; one is semi-infinite arrays and the other is gap arrays. In the case of semi-infinite arrays, continuous square arrays of nanoparticles were fabricated within the $100 \times 100 \mu\text{m}^2$ area with various grid spacings (D). Table 1 summarizes all the semi-infinite arrays fabricated for this study. Nanoparticle arrays with $5 \mu\text{m}$ grid spacing were also fabricated in order to obtain optical properties of “isolated” nanoparticles. At this grid spacing, dipole interaction between nanoparticles is negligible. In the case of the gap array, vacant sites were introduced within the $100 \times 100 \mu\text{m}^2$ square array of nanoparticles as shown in Figure 1C. In the gap arrays, each unit block consists of a certain number of nanoparticles with fixed grid spacing, and they are separated by a certain gap dimension. Figure 1D shows the diagram of gap arrays with 3×3 blocks (three particles per block edge) and gap size of 2. Gray particles in the diagram stand for vacant sites. For the

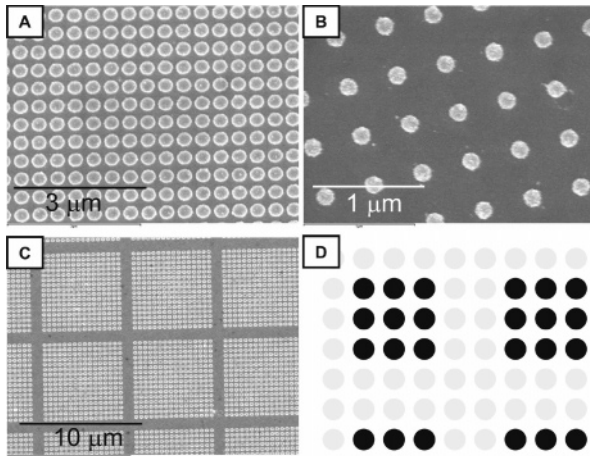


Figure 1. SEM images of two-dimensional square arrays of cylindrical nanoparticles. (A) $d = 339$ nm nanoparticles. (B) $d = 163$ nm nanoparticles. (C) Gap array of $d = 339$ nm nanoparticles (16 particles per block edge and gap of 2 particles). (D) Diagram of gap arrays with 3×3 blocks and gap size of 2. Gray particles in the diagram stand for vacant sites.

TABLE 1: Characteristics of Semi-infinite Square Arrays

diameter (nm)	grid spacing (nm)
339 ^a	400, 450, 475, 500, 525, 550, 600, 650, 700, 800, 900, 5000
163 ^b	450, 475, 500, 525, 550, 600, 800, 900

^a Error is ± 6 nm. ^b Error is ± 4 nm.

TABLE 2: Characteristics of Gap Arrays

diameter (nm)	grid spacing (nm)	block size ^a	gap size ^a
Gap Array 1 ^b			
339	400, 450	$2 \times 2, 3 \times 3, 4 \times 4$	1, 2
339	400, 450	$8 \times 8, 16 \times 16, 24 \times 24$	1, 2, 8
339	400, 450	40×40	1
339	5000	1×1	n/a
339	400/450	semi-infinite ($250 \times 250/222 \times 222$)	0
Gap Array 2 ^c			
163	450	$2 \times 2, 3 \times 3, 4 \times 4$	1, 2
163	450	$8 \times 8, 16 \times 16, 24 \times 24$	1, 2, 8
163	450	40×40	1
163	450	semi-infinite (222×222)	0

^a Number of particles. ^b Error is ± 6 nm. ^c Error is ± 4 nm.

large cylinders, gap arrays of 400 and 450 nm grid spacing were fabricated (gap array 1), and for the small cylinders, gap arrays of 450 nm grid spacing were fabricated (gap array 2). Various numbers of particles in single block and various gap sizes were fabricated for both large and small cylinders. All the gap arrays reported in this paper are summarized in Table 2.

B. Extinction Measurements. Extinction spectra were collected on an Ocean Optics USB2000 fiber-coupled spectrometer for the 400–1000 nm region and a fiber-coupled near-IR spectrometer (NIR 128L-1.7T1-USB, Control Development) for the 900–1700 nm region. The spectra over this wide region have a slight mismatch near 900 nm, signifying where one spectrometer ends and the other begins. The experimental setup for the extinction measurements is described in detail elsewhere.³⁵ Briefly, white light from a tungsten–halogen lamp light source was fiber-coupled with a $100 \mu\text{m}$ fiber to a +40 mm focal length achromatic collimating lens. The collimated beam was then polarized by a Glan-Taylor calcite polarizer with 5 mm aperture and focused onto the sample by a +12.7 mm focal

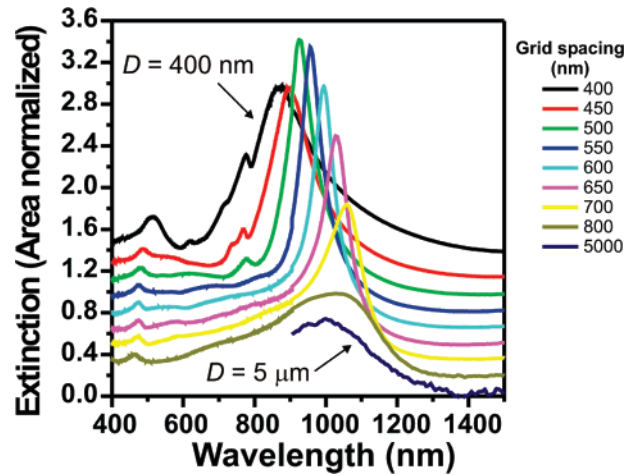


Figure 2. Nanoparticle area-normalized extinction spectra of 2D square arrays of $d = 339$ nm nanoparticles (large cylinders). Grid spacing ranges from 400 nm to $5 \mu\text{m}$ from top to bottom. All spectra are shown with an offset of 0.15 for clarity. In the case of isolated particle ($D = 5 \mu\text{m}$), only the spectrum obtained by near-IR spectrometry is available.

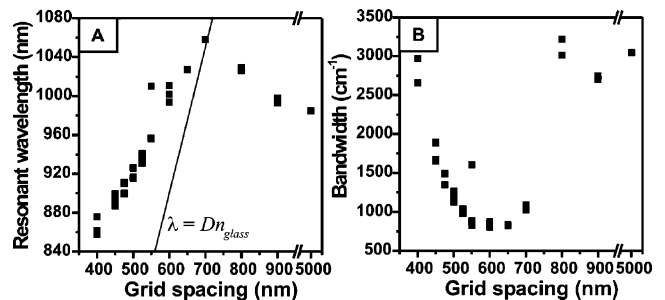


Figure 3. (A) Resonant wavelength and (B) bandwidth versus grid spacing for 2D semi-infinite arrays of $d = 339$ nm nanoparticles (large cylinders). The light line $\lambda = Dn_{\text{glass}}$ is shown as a black solid line in panel A. λ is wavelength, D is grid spacing, and n_{glass} is the refractive index of glass ($n_{\text{glass}} = 1.5$).

length achromatic lens with the optic axis normal to the sample surface. Transmitted light was collected by an infinity-corrected $10\times$ Nikon microscope objective ($\text{NA} = 0.30$) at a working distance of 16.0 mm and focused into a $600 \mu\text{m}$ fiber that couples into the spectrometer. The white light spot size on the sample was scanned with a straight edge and was close to Gaussian with a $20 \mu\text{m}$ diameter at full width at half-maximum (fwhm).

The sample was mounted on two computer-controlled micro-translational stages (M-111.1DG, Physik Instrumente) to form an x – y system with a 50 nm step size. The x – y stage system is fixed on the manual vertical linear stage (MVN50, Newport Corp.) and manual rotational stage (M-UTR120A, Newport Corp.). All the samples were studied under a stream of dry nitrogen. The reference measurement was obtained by scanning into a nearby region of the glass substrate.

III. Results and Discussion

A. Semi-Infinite Arrays. The extinction spectra of semi-infinite 2D arrays of large cylinders ($d = 339$ nm) with various grid spacings are depicted in Figure 2. The resonant wavelength and bandwidth of the arrays vary with grid spacing. The resonant wavelength is plotted versus grid spacing in Figure 3A. Multiple points for each grid distance are the data obtained from multiple pads that were fabricated with the same grid spacing. The resonant wavelength red-shifts as the grid spacing increases until 700 nm, where it shows maximum red shift. This grid spacing

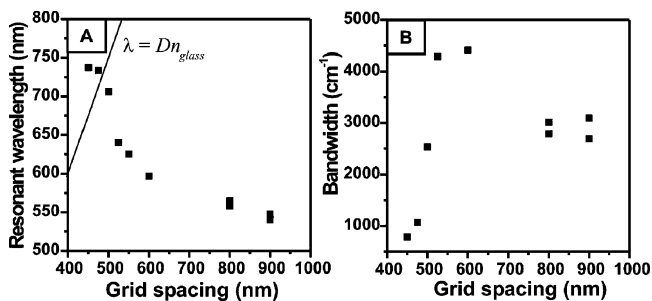


Figure 4. (A) Resonant wavelength and (B) bandwidth versus grid spacing for 2D semi-infinite arrays of $d = 163$ nm nanoparticles (small cylinders). The light line $\lambda = Dn_{\text{glass}}$ is shown as a black solid line in panel A. λ is wavelength, D is grid spacing, and n_{glass} is refractive index of glass ($n_{\text{glass}} = 1.5$).

will be called critical grid spacing (D_{crit}). The red shift of resonant wavelength before D_{crit} is consistent with the previous observations by Van Duyne and co-workers³⁶ and the theoretical calculations by Schatz and co-workers.^{36,40,42} In our case, the isolated particle resonance is at much longer wavelengths than the arrays, with $D < 500$ nm, where there are strong interactions between the large particles due to their large dipole and relatively close spacing. After D_{crit} , the resonant wavelength blue-shifts and converges to that of the isolated nanoparticle. As shown in Figure 3A, D_{crit} is observed where the plot of resonant wavelength versus grid spacing intersects with the light line given by $\lambda = Dn_{\text{glass}}$, where λ is wavelength and n_{glass} is the refractive index of glass substrate ($n_{\text{glass}} = 1.5$). The bandwidth of the plasmon resonance is plotted versus grid spacing in Figure 3B. The minimum bandwidth of 806 cm^{-1} is shown at 650 nm grid spacing that is 50 nm smaller than the D_{crit} . This bandwidth corresponds to a plasmon lifetime of 6.6 fs. All these observations are consistent with the previous reports for cylindrical nanoparticle arrays³³ and L-shaped nanoparticle arrays.³⁵ Ausenegg and co-workers³³ explained the observation with the model proposed by Meier et al.³⁷ The narrow plasmon resonance at the grid spacing slightly smaller than D_{crit} was explained by the large local optical fields due to an almost in-phase addition of the scattered light fields of neighboring particles while the grating order is evanescent.³³ At D_{crit} , the grating order changes from evanescent to radiating at grazing angle, where strong damping occurs, which broadens the bandwidth.³³

Some additional features are shown in the extinction spectra of Figure 2. There is a small band in the 460–520 nm region, and it can be a quadrupole or a higher-order multipole band. At the closest grid spacing, this small band red-shifts and its intensity increases, which is consistent with the previous observation for L-shaped nanoparticle arrays.³⁵ In the case of grid spacings smaller than 550 nm, a small additional band is observed in the 770–780 nm region, but the origin of this band is not clear.

The resonant wavelength and bandwidth of the dipole band of small cylinder arrays ($d = 163$ nm) are plotted versus grid spacing in Figure 4. In the case of small cylinders, D_{crit} is about 475–500 nm and it is smaller than D_{crit} of large cylinder arrays (700 nm); this shift is because the resonant wavelength of the small cylinder is blue-shifted relative to the large cylinder. The resonant wavelength of an isolated nanoparticle is 985 nm for the large cylinder. In the case of the small cylinder, an isolated nanoparticle array did not survive the fabrication process. However, if we assume that the optical properties of a 900 nm grid spacing array approaches to that of isolated nanoparticle sufficiently, the resonant wavelength of the isolated particle is about 545 nm.

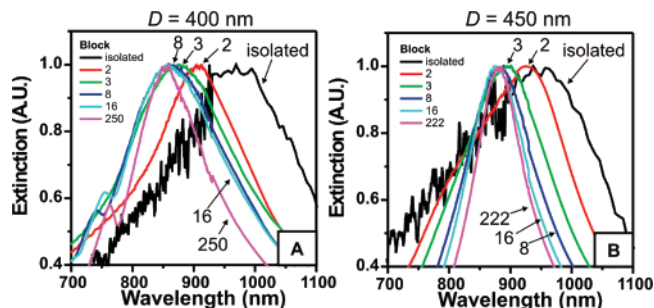


Figure 5. Extinction spectra of gap array 1 ($d = 339$ nm) for (A) $D = 400$ nm and (B) $D = 450$ nm. Extinction spectra of isolated particle; 2×2 , 3×3 , 8×8 , and 16×16 blocks with gap dimension of 1; and semi-infinite arrays are plotted with black, red, green, blue, cyan, and purple lines, respectively. Each spectrum is normalized to the height of the extinction maximum.

B. Gap Arrays. In order to monitor how the number of interacting particles affects the optical properties of finite 2D arrays, we fabricated two different types of gap arrays. One gap array consists of large cylinders with 400 and 450 nm grid spacing (gap array 1 in Table 2), and the other consists of small cylinders with 400 nm grid spacing (gap array 2 in Table 2). In the case of gap arrays 1, their grid spacing is much smaller than D_{crit} of the semi-infinite array with the same nanoparticle size as shown in Figure 3, where D_{crit} of the semi-infinite array is 700 nm. In the case of gap arrays 2, their grid spacing is still smaller than D_{crit} of the semi-infinite array with the same nanoparticle size, but they are similar. D_{crit} of this semi-infinite array is about 475–500 nm as shown in Figure 4. Since the grid spacing is smaller than D_{crit} for both arrays, their grating order is evanescent; that is, the reciprocal lattice vector ($2\pi/D$) is larger than the wavevector of the resonant wavelength within a glass medium ($2\pi n_{\text{glass}}/\lambda$). However, in the case of the semi-infinite array of large cylinders with $D = 400$ and 450 nm, the resonant wavelength is blue-shifted from the corresponding isolated nanoparticle resonance (Figure 3A), whereas in the case of small cylinder arrays with $D = 450$ nm, the resonant wavelength is red-shifted from the corresponding isolated nanoparticle resonance (Figure 4A). For the two different cases, we constructed 2D square arrays with finite nanoparticle numbers. The numbers of nanoparticles were varied from an isolated nanoparticle (particle number = 1) to the semi-infinite arrays (particle number = 250×250 for $D = 400$ nm, 222×222 for $D = 450$ nm) as summarized in Table 2, and we monitored the modification of optical properties. Data for an isolated nanoparticle for the small cylinder were not available; therefore the data for the semi-infinite array with $D = 900$ nm will approximate the isolated particle data in our discussion.

The extinction spectra of selected arrays from gap array 1 with large particles ($d = 339$ nm) and $D = 400$ and 450 nm are depicted in Figure 5. The extinction spectra of isolated particle; 2×2 , 3×3 , 8×8 , and 16×16 blocks with gap dimension of 1; and semi-infinite arrays are plotted with black, red, green, blue, cyan, and purple lines, respectively. Each spectrum is normalized to the height of the extinction maximum. The resonant wavelength blue-shifts as the number of nanoparticles in the block increases for both $D = 400$ and 450 nm arrays. The resonant wavelengths of gap array 1 with $D = 400$ and 450 nm are shown in Figure 6, panels A and C, respectively. The resonant wavelength of the isolated nanoparticle is 955–965 nm and that of the semi-infinite array is 856 nm for $D = 400$ nm and 874–884 nm for $D = 450$ nm. The slight difference in resonance position with the data in Figure 4 might be because of the small difference in each sample that comes from the

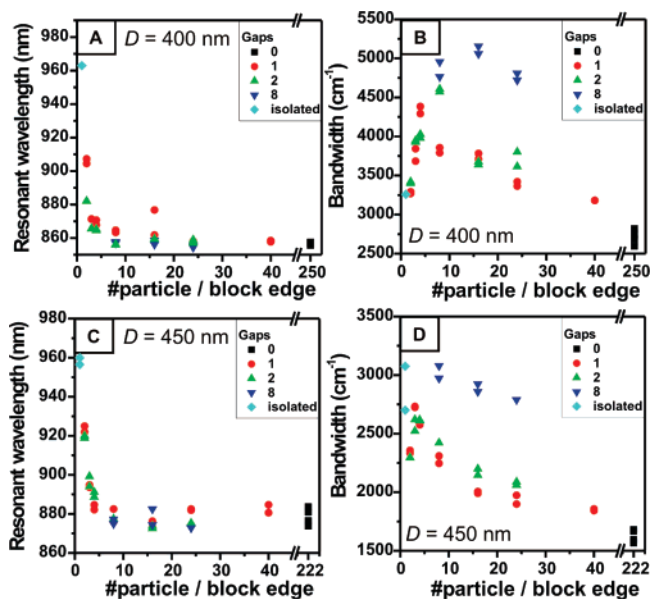


Figure 6. Resonant wavelength and bandwidth of gap array 1 samples ($d = 339$ nm) versus the number of particles per block edge: (A, B) gap arrays with $D = 400$ nm; (C, D) gap arrays with $D = 450$ nm. Data for semi-infinite particle arrays are plotted with black squares; data with gaps corresponding to 1, 2, and 8 particles are plotted with red circles, green triangles, and blue inverted triangles, respectively. Data for isolated particles are plotted with cyan diamonds.

imperfection of the fabrication. As the number of particles increases, the resonant wavelength blue-shifts and it approaches that of the semi-infinite array. The formation of a 2×2 block induces a large blue shift from the isolated nanoparticle resonance, ~ 60 nm for $D = 400$ nm and ~ 40 nm for $D = 450$ nm, followed by a gradual blue shift approaching the semi-infinite array resonance as the number of nanoparticles increases. The resonance of 16×16 nanoparticles approached that of a semi-infinite array and there is little change in resonant wavelength for larger blocks. These trends show the importance of more particles creating more interparticle interactions and correlated resonance shifts. However, the size of gap does not seem to play a significant role in the resonant wavelength. Except for the 2×2 block with $D = 400$ nm, the other blocks show similar resonant wavelengths for different gap dimensions.

The extinction spectra of selected arrays from gap array 2 with smaller particles ($d = 163$ nm) are depicted in Figure 7. The extinction spectra of the isolated particle; 2×2 , 3×3 , 8×8 , and 16×16 blocks with gap dimension of 1; and semi-infinite arrays are plotted with black, red, green, blue, cyan, and purple lines, respectively. The resonant wavelength red-shifts as the number of nanoparticles in the block increases and approaches the resonance of the semi-infinite array. The resonant wavelengths of gap array 2 are plotted in Figure 8. The resonant wavelength of the isolated nanoparticle is 540–548 nm and that of the semi-infinite array is 737–771 nm. As the number of particles increases, the resonant wavelength red-shifts and approaches that of the semi-infinite array. A red shift of 140 nm from the isolated nanoparticle resonance is observed with the formation of a 2×2 block, followed by a gradual red shift approaching the semi-infinite array resonance as the number of nanoparticles increases. Here again, the resonance of 16×16 nanoparticles approached that of semi-infinite array and the size of gap does not play a significant role in the resonant wavelength.

The bandwidth of the gap array shows complicated behaviors. The plasmon bandwidth of gap array 1 with $D = 400$ and 450

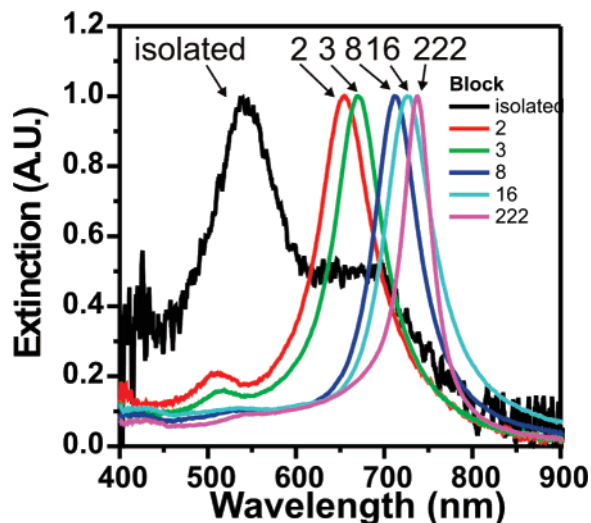


Figure 7. Extinction spectra of gap array 2 ($d = 163$ nm). Extinction spectra of isolated particle; 2×2 , 3×3 , 8×8 , and 16×16 blocks with gap dimension of 1; and semi-infinite arrays are plotted with black, red, green, blue, cyan, and purple lines, respectively. Each spectrum is normalized to the height of the extinction maximum.

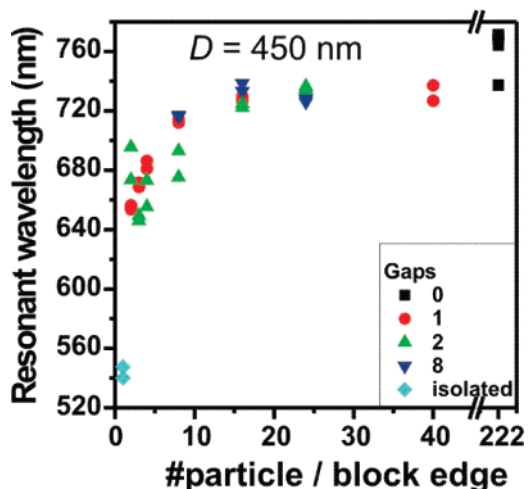


Figure 8. Resonant wavelength of gap array 2 samples ($d = 163$ nm, $D = 450$ nm) vs the number of particles per block edge. Data for semi-infinite particle arrays are plotted with black squares; data with gaps corresponding to 1, 2, and 8 particles are plotted with red circles, green triangles, and blue inverted triangles, respectively. Data for isolated particles are plotted with cyan diamonds.

nm are shown in Figure 6, panels B and D, respectively. For a fixed gap dimension, the bandwidth increases as the number of nanoparticles increases up to a certain block dimension, and then it decreases and approaches that of semi-infinite array; at no spacing is the bandwidth less than the semi-infinite array. For the $D = 400$ nm sample, the maximum bandwidth is observed at 4×4 , 8×8 , and 16×16 blocks for gap dimensions of 1, 2, and 8, respectively; and for the $D = 450$ nm sample, the maximum bandwidth is observed at 3×3 and 4×4 blocks for gap dimensions of 1 and 2, respectively. For a fixed block dimension, a larger gap results in broader bandwidth with some exceptions. The blocks with gap dimension of 8 show large bandwidth compared to those with gap dimensions of 1 and 2 for both $D = 400$ and 450 nm. They are fabricated on different substrates from the other gap arrays, and therefore a slight variation of nanoparticles that came from the imperfection of the sample fabrication might cause the large deviation in bandwidth. Generally, for the samples prepared with identical geometric parameters, the bandwidth shows larger

deviation than the resonance wavelength. However, it is still possible that the observation is real and not an artifact. For the large gap of 8, each block is isolated and there is no interaction between blocks. On the other hand, in the case of the small gap of 1 and 2, each block is quite close and dipole interactions among those blocks are possible because of the high polarizability of the large nanoparticles, which narrows the bandwidth. In order to verify this hypothesis, more samples with various gap dimensions between 2 and 8 should be tested.

In the case of gap array 2, samples showed larger deviation in bandwidth for different preparations (not shown), even though the resonance wavelengths had much less fluctuation. More experiments and theoretical modeling are required to explore the effect on the plasmon bandwidth more precisely.

IV. Conclusion

We measured the optical properties of finite 2D arrays of silver cylindrical nanoparticles of variable size and gap spacing. The change in resonance wavelength from a single particle to a 2×2 particle and larger arrays is substantial, and the series of increasing block sizes shows the effects of more particle interactions in eventually reaching the resonance properties of semi-infinite arrays. In the case of gap array 1 of large-diameter nanoparticles, the resonant wavelength of the 2×2 block blue-shifts from that of isolated particles, and as the block dimension increases, the resonant wavelength keeps blue-shifting and converges to that of a semi-infinite array. In the case of gap array 2 of small-diameter nanoparticles, the resonant wavelength of the 2×2 particle blocks red-shifts from that of isolated particles, and as the block dimension increases, the resonant wavelength keeps red-shifting and converges to that of a semi-infinite array. In both cases, the size of the gap does not seem to play a significant role in the resonant wavelength, although the noise of the data might be obscuring subtle trends. In the case of gap array 1, as the number of nanoparticles in the block increases, the bandwidth of the block resonance increases up to a certain block dimension and then decreases to converge to the bandwidth of the semi-infinite array resonance. Larger gaps between the blocks show larger bandwidth for the fixed block dimension, but more study is required to explore the effect of gap dimension on the bandwidth of the array resonance in detail.

These results on small arrays provide data to test theoretical models of small arrays and varying gaps between arrays. The experimental resonances for progressively increasing array sizes show systematic resonance shifts consistent with increasing numbers of particles, but the bandwidth trends require models and more experiments to obtain better insight into trends.

Acknowledgment. We gratefully acknowledge support from the Air Force Office of Scientific Research (MURI Program Grant F49620-02-1-0381), the DTRA JSTO Program (Grant FA9550-06-1-0558), and the National Science Foundation (EEC-0647560, CHE-0414554, DMR-0520513). Samples were fabricated at the Michigan Nanofabrication Facility (MNF), which is part of the National Nanotechnology Infrastructure Network (NNIN).

References and Notes

- Haes, A. J.; Van Duyne, R. P. *J. Am. Chem. Soc.* **2002**, *124*, 10596.
- Zhao, J.; Zhang, X.; Yonzon, C. R.; Haes, A. J.; Van Duyne, R. P. *Nanomedicine* **2006**, *1*, 219.
- Henglein, A.; Meisel, D. *J. Phys. Chem. B* **1998**, *102*, 8364.
- Elghanian, R.; Storhoff, J. J.; Mucic, R. C.; Letsinger, R. L.; Mirkin, C. A. *Science* **1997**, *277*, 1078.
- Dirix, Y.; Bastiaansen, C.; Caseri, W.; Smith, P. *Adv. Mater.* **1999**, *11*, 223.
- Ebbesen, T. W.; Lezec, H. J.; Ghaemi, H. F.; Thio, T.; Wolff, P. A. *Nature* **1998**, *391*, 667.
- Knoll, W. *Annu. Rev. Phys. Chem.* **1998**, *49*, 569.
- Quinten, M.; Leitner, A.; Krenn, J. R.; Aussenegg, F. R. *Opt. Lett.* **1998**, *23*, 1331.
- Brongersma, M. L.; Hartman, J. W.; Atwater, H. A. *Phys. Rev. B* **2000**, *62*, R16356.
- Egusa, S.; Liao, Y. H.; Scherer, N. F. *Appl. Phys. Lett.* **2004**, *84*, 1257.
- Freeman, R. G.; Grabar, K. C.; Allison, K. J.; Bright, R. M.; Davis, J. A.; Guthrie, A. P.; Hommer, M. B.; Jackson, M. A.; Smith, P. C.; Walter, D. G.; Natan, M. J. *Science* **1995**, *267*, 1629.
- McFarland, A. D.; Young, M. A.; Dieringer, J. A.; Van Duyne, R. P. *J. Phys. Chem. B* **2005**, *109*, 11279.
- Kahl, M.; Voges, E.; Kostrewa, S.; Viets, C.; Hill, W. *Sens. Actuators, B* **1998**, *51*, 285.
- Bohren, C. F.; Huffman, D. R. *Absorption and Scattering of Light by Small Particles*; Wiley-VCH: Weinheim, Germany, 2004.
- Haynes, C. L.; Van Duyne, R. P. *J. Phys. Chem. B* **2001**, *105*, 5599.
- Chan, G. H.; Zhao, J.; Hicks, E. M.; Schatz, G. C.; Van Duyne, R. P. *Nano Lett.* **2007**, *7*, 1947.
- Jensen, T. R.; Duval, M. L.; Kelly, K. L.; Lazarides, A. A.; Schatz, G. C.; Van Duyne, R. P. *J. Phys. Chem. B* **1999**, *103*, 9846.
- Kelly, K. L.; Coronado, E.; Zhao, L.; Schatz, G. C. *J. Phys. Chem. B* **2003**, *107*, 668.
- Rechberger, W.; Hohenau, A.; Leitner, A.; Krenn, J. R.; Lamprecht, B.; Aussenegg, F. R. *Opt. Commun.* **2003**, *220*, 137.
- Su, K.-H.; Wei, Q.-H.; Zhang, X.; Mock, J. J.; Smith, D. R.; Schultz, S. *Nano Lett.* **2003**, *3*, 1087.
- Gunnarsson, L.; Rindzevicius, T.; Prikulis, J.; Kasemo, B.; Käll, M.; Zou, S.; Schatz, G. C. *J. Phys. Chem. B* **2005**, *109*, 1079.
- Tamaru, H.; Kuwata, H.; Miyazaki, H. T.; Miyano, K. *Appl. Phys. Lett.* **2002**, *80*, 1826.
- Atay, T.; Song, J.-H.; Nurmikko, A. V. *Nano Lett.* **2004**, *4*, 1627.
- Jain, P. K.; Huang, W.; El-Sayed, M. A. *Nano Lett.* **2007**, *7*, 2080.
- Nordlander, P.; Prodan, E. *Nano Lett.* **2004**, *4*, 2209.
- Hohenester, U.; Krenn, J. *Phys. Rev. B* **2005**, *72*, 195429.
- Schmeits, M.; Dambly, L. *Phys. Rev. B* **1991**, *44*, 12706.
- Sönnichsen, C.; Reinhard, B. M.; Liphardt, J.; Alivisatos, A. P. *Nat. Biotechnol.* **2005**, *23*, 741.
- Reinhard, B. M.; Siu, M.; Agarwal, H.; Alivisatos, A. P.; Liphardt, J. *Nano Lett.* **2005**, *5*, 2246.
- Maier, S. A.; Brongersma, M. L.; Kik, P. G.; Atwater, H. A. *Phys. Rev. B* **2002**, *65*, 193408.
- Sweatlock, L. A.; Maier, S. A.; Atwater, H. A.; Penninkhof, J. J.; Polman, A. *Phys. Rev. B* **2005**, *71*, 235408.
- Hicks, E. M.; Zou, S.; Schatz, G. C.; Spears, K. G.; Van Duyne, R. P.; Gunnarsson, L.; Rindzevicius, T.; Kasemo, B.; Käll, M. *Nano Lett.* **2005**, *5*, 1065.
- Lamprecht, B.; Schider, G.; Lechner, R. T.; Ditlbacher, H.; Krenn, J. R.; Leitner, A.; Aussenegg, F. R. *Phys. Rev. Lett.* **2000**, *84*, 4721.
- Féridj, N.; Laurent, G.; Aubard, J.; Lévi, G.; Hohenau, A.; Krenn, J. R.; Aussenegg, F. R. *J. Chem. Phys.* **2005**, *123*, 221103.
- Sung, J.; Hicks, E. M.; Van Duyne, R. P.; Spears, K. G. *J. Phys. Chem. C* **2007**, *111*, 10368.
- Haynes, C. L.; McFarland, A. D.; Zhao, L.; Van Duyne, R. P.; Schatz, G. C.; Gunnarsson, L.; Prikulis, J.; Kasemo, B.; Käll, M. *J. Phys. Chem. B* **2003**, *107*, 7337.
- Meier, M.; Wokaun, A.; Liao, P. F. *J. Opt. Soc. Am. B* **1985**, *2*, 931.
- Zou, S.; Janel, N.; Schatz, G. C. *J. Chem. Phys.* **2004**, *120*, 10871.
- Zou, S.; Schatz, G. C. *J. Chem. Phys.* **2004**, *121*, 12606.
- Zhao, L.; Kelly, K. L.; Schatz, G. C. *J. Phys. Chem. B* **2003**, *107*, 7343.
- Maier, S. A.; Kik, P. G.; Atwater, H. A. *Appl. Phys. Lett.* **2002**, *81*, 1714.
- Zou, S.; Zhao, L.; Schatz, G. C. *Proc. SPIE-Int. Soc. Opt. Eng.* **2003**, *5221*, 174.
- Wei, Q.-H.; Su, K.-H.; Durant, S.; Zhang, X. *Nano Lett.* **2004**, *4*, 1067.
- Bouhelier, A.; Bachelot, R.; Im, J. S.; Wiederrecht, G. P.; Lerondel, G.; Kostcheev, S.; Royer, P. *J. Phys. Chem. B* **2005**, *109*, 3195.
- Ng, M.-Y.; Liu, W.-C. *Opt. Express* **2006**, *14*, 4504.
- Brockman, J. M.; Nelson, B. P.; Corn, R. M. *Annu. Rev. Phys. Chem.* **2000**, *51*, 41.